

A New Candidate Transitional Millisecond Pulsar in the Subluminous Disk State: 4FGL J0407.7–5702

Jessie M. Miller , Samuel J. Swihart , Jay Strader , Ryan Urquhart , Elias Aydi , Laura Chomiuk , Kristen C. Dage , Adam Kawash , Laura Shishkovsky , and Kirill V. Sokolovsky , and Kirill V. Sokolovsky , and Laura Chomiuk , and Laura Chomiuk , Kristen C. Dage , Adam Kawash , Laura Shishkovsky , and Kirill V. Sokolovsky , and Laura Chomiuk , and Kirill V. Sokolovsky , and Laura Chomiuk , and Kirill V. Sokolovsky , and Kirill V. Sokolovsky , and Laura Chomiuk , and Kirill V. Sokolovsky , and Kirill V. Sokolovsky , and Laura Chomiuk , and Kirill V. Sokolovsky , and Kirill V. Sokolovsk

² Sternberg Astronomical Institute, Moscow State University, Universitetskii pr. 13, 119992 Moscow, Russia Astro Space Center of Lebedev Physical Institute, Profsoyuznaya St. 84/32, 117997 Moscow, Russia Received 2020 August 21; revised 2020 September 18; accepted 2020 September 18; published 2020 November 20

Abstract

We report the discovery of a variable optical and X-ray source within the error ellipse of the previously unassociated Fermi Large Area Telescope γ -ray source 4FGL J0407.7–5702. A 22 ks observation from XMM-Newton/European Photon Imaging Camera (EPIC) shows an X-ray light curve with rapid variability and flaring. The X-ray spectrum is well fit by a hard power law with $\Gamma=1.7$. Optical photometry taken over several epochs is dominated by aperiodic variations of moderate amplitude. Optical spectroscopy with Southern Astrophysical Research (SOAR) and Gemini reveals a blue continuum with broad and double-peaked H and He emission, as expected for an accretion disk around a compact binary. Overall, the optical, X-ray, and γ -ray properties of 4FGL J0407.7–5702 are consistent with a classification as a transitional millisecond pulsar in the subluminous disk state. We also present evidence that this source is more distant than other confirmed or candidate transitional millisecond pulsar binaries, and that the ratio of X-ray to γ -ray flux is a promising tool to help identify such binaries, indicating that a more complete census for these rare systems is becoming possible.

Unified Astronomy Thesaurus concepts: Neutron stars (1108); Gamma-rays (637)

Supporting material: data behind figures

1. Introduction

Transitional millisecond pulsars (tMSPs) form a unique subclass of stellar compact binary system containing a neutron star and a low-mass, nondegenerate companion. These binaries are identified by their observed transitions between a low-mass X-ray binary-like state and a rotation-powered radio millisecond pulsar state on timescales of weeks to years. To date, only three systems have been observed to undergo such transitions: PSR J1023+0038 (Archibald et al. 2009) and XSS J12270–4859 (Bassa et al. 2014; Roy et al. 2015) in the Galactic field, and IGR J18245–2452 (Papitto et al. 2013) in the globular cluster M28.

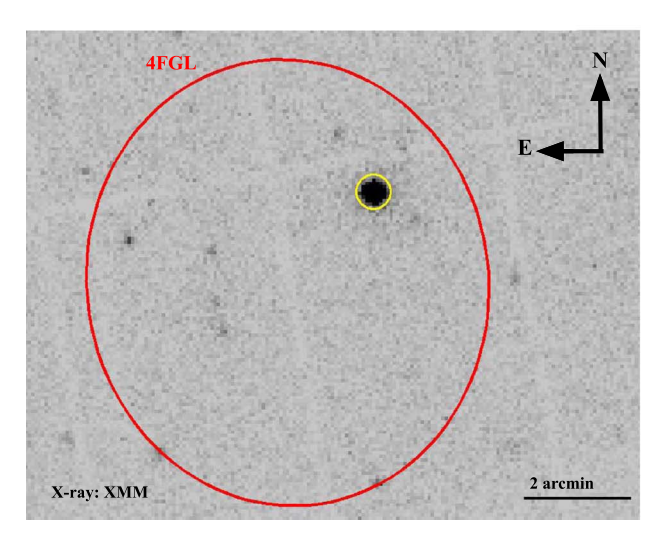
In addition to these class-defining transitions, tMSPs show other distinctive characteristics, especially in the disk state. Their typical 1–10 keV X-ray luminosities are $L_{\rm X}\sim 10^{33-34}\,{\rm erg\,s^{-1}}$ (de Martino et al. 2013; Papitto et al. 2013; Patruno et al. 2014). This is much lower than the typical values of $L_{\rm X}\gtrsim 10^{36}\,{\rm erg\,s^{-1}}$ observed for persistent or outbursting transient neutron star low-mass X-ray binaries (van Paradijs 1998). Hence, this $L_{\rm X}\sim 10^{33-34}\,{\rm erg\,s^{-1}}$ state is also called the subluminous disk state. A single tMSP (IGR J18245–2452; Papitto et al. 2013) has been observed at the outburst $L_{\rm X}$ of a few $\times 10^{36}\,{\rm erg\,s^{-1}}$ traditionally seen for accreting millisecond X-ray pulsars (Patruno & Watts 2012). While it is uncertain what fraction of tMSPs show such outbursts, this case shows that it is a possible alternative route to tMSP discovery.

The X-ray light curves show variability on a range of amplitudes and timescales. In the three confirmed tMSPs this variability exhibits remarkable "mode switching": abrupt changes between distinct low and high modes (de Martino et al. 2013; Linares et al. 2014; Bogdanov et al. 2015) that

differ by a factor of $\sim 5-10$ in X-ray luminosity, with occasional more luminous flares. During the high mode there is evidence of X-ray and optical pulsations (Archibald et al. 2010, 2015; Papitto et al. 2015; Ambrosino et al. 2017). In the low mode X-ray pulsations are not seen, and instead radio continuum emission is observed, likely from synchrotron-emitting bubbles produced close to the neutron star (Bogdanov et al. 2018).

A self-consistent model of these observations has not yet been firmly established. Indeed it is unclear whether (i) the disk state is accretion powered, with some accreted material reaching the surface of the neutron star and the rest possibly ejected in a propeller (Bogdanov et al. 2015; Papitto & Torres 2015) or maintained in a "trapped disk" (D'Angelo & Spruit 2012), or (ii) whether the disk state is instead rotation powered, with the X-ray emission (including the X-ray pulsations) due to shocks from the pulsar wind occurring just outside the light cylinder (Ambrosino et al. 2017; Papitto et al. 2019; Veledina et al. 2019) or at a larger radius (Takata et al. 2014). Notably, timing observations of PSR J1023+0038 show that the pulsar spin-down rate increases by $\sim 27\%$ in the subluminous disk state compared to the radio pulsar state (Jaodand et al. 2016). This suggests that the pulsar wind is enhanced during the disk state, rather than being suppressed, as might be expected if accretion is occurring. The detection of radio pulsations in the disk state could help settle the question, but these have not been detected in the subluminous disk state of any of the confirmed tMSPs despite extensive searches (Hill et al. 2011; Papitto et al. 2013; Stappers et al. 2014; Jaodand et al. 2016).

In another departure from typical low-mass X-ray binary phenomenology, the two field tMSPs show enhanced GeV γ -



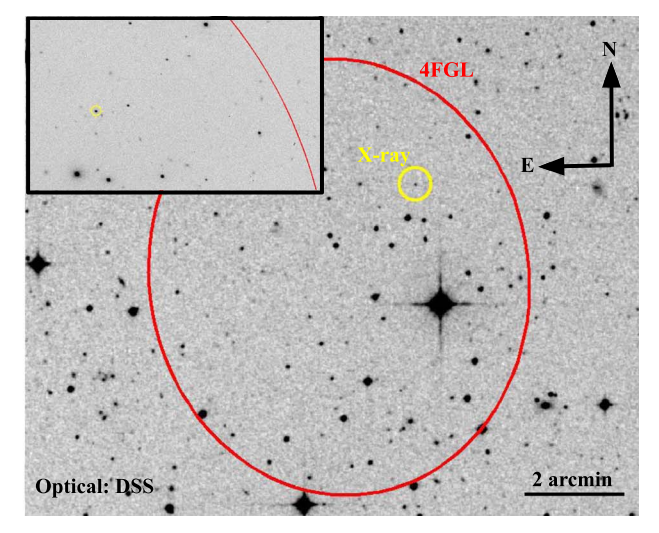


Figure 1. Left: XMM-Newton/EPIC X-ray image of the field of 4FGL J0407.7–5702. The 95% 4FGL error ellipse is in red, and the candidate X-ray/optical counterpart is circled in yellow. Right: Red Digitized Sky Survey image of the field with the X-ray source marked in yellow. The inset is a zoomed-in unfiltered optical image taken with the SOAR telescope, with the source again marked with a yellow circle.

ray emission in the subluminous disk state: they are brighter by a factor of a few compared to the millisecond pulsar state (Stappers et al. 2014; Johnson et al. 2015). Besides the known tMSPs (and the candidate tMSPs selected via γ -ray emission), no other low-mass X-ray binary at $L_{\rm X} \lesssim 10^{35}\,{\rm erg\,s^{-1}}$ has shown persistent γ -ray emission, including a number of relatively nearby accreting millisecond X-ray pulsars (Torres & Li 2020).

Regardless of whether the disk state in tMSPs is actually powered by accretion, there is strong evidence from the optical that a disk is indeed present. Optical spectra in this state are dominated by a warm continuum and the double-peaked H and He emission lines characteristic of an accretion disk around a compact object (Bond et al. 2002; de Martino et al. 2014). In the MSP state, these optical signatures of a disk disappear (Thorstensen & Armstrong 2005; de Martino et al. 2015).

Unlike the apparently unique subluminous disk state, tMSPs in the pulsar state have multiwavelength properties comparable to the other compact binaries with nondegenerate companions. These systems are typically called "redbacks" when the companion mass is $\gtrsim 0.1 M_{\odot}$ (Roberts 2013). The X-ray emission in redbacks is usually dominated by a hard intrabinary shock modulated on the orbital period (Linares 2014; Roberts et al. 2014). Typical pulsar searches strongly select against eclipsing pulsars such as redbacks, and targeted follow-up of new γ -ray sources discovered with the Fermi Large Area Telescope (LAT) has been the most important tool in substantially increasing the known sample of field redbacks (Ray et al. 2012; Roberts 2013).

Redbacks are not mere curiosities: as a population they have among the highest neutron star masses known for any subclass of millisecond pulsars (Strader et al. 2019), and some are among the fastest spinning pulsars known (Patruno et al. 2017). Since all tMSPs are redbacks it is natural to wonder whether the converse holds, but despite intensive searches (e.g., Torres et al. 2017) no other field redbacks have been observed to transition to or from the pulsar state.

Instead, new candidate tMSPs have been identified using the distinguishing characteristics of the class in the subluminous disk state, including γ -ray emission, variable X-ray emission with $L_{\rm X}\sim 10^{33}$ – $10^{34}\,{\rm erg\,s^{-1}}$, and evidence for a disk. The

three convincing candidates found this way are 3FGL (Bogdanov & Halpern 2015), J1544.6-1125 3FGL J0427.9-6704 (Strader et al. 2016), and J110926.4-650224 (Coti Zelati et al. 2019). This tMSP discovery route, while very useful, is certainly incomplete: some other sources have X-ray luminosities and variability properties somewhat similar to tMSPs in the subluminous disk state, but perhaps have not been detected as γ -ray sources due to their distances or confused sky locations (e.g., Degenaar et al. 2014; Heinke et al. 2015). It is plausible that some of these sources are indeed tMSPs and could be identified as such with future multiwavelength observations.

Here we present the discovery and characterization of a compact binary within the error ellipse of the Fermi-LAT γ -ray source 4FGL J0407.7–5702. We show this source has X-ray and optical properties similar to the known tMSPs in the subluminous disk state and hence is a strong tMSP candidate.

2. Observations

2.1. The γ -Ray Source and Optical Discovery

The candidate X-ray/optical counterpart was discovered as part of our ongoing program to search for new compact binaries among previously unassociated Fermi-LAT γ -ray sources (Figure 1). We are focused in particular on possible counterparts that are both optical variables and X-ray sources, since this preferentially selects for compact binaries over unrelated contaminants.

The focus of this paper is on an X-ray/optical source at the edge of the 68% error ellipse—and hence well within the 95% error ellipse—of the LAT 4FGL-DR2 (10 yr) source 4FGL J0407.7–5702 (Ballet et al. 2020). The 95% error ellipse is not too far from circular, with a mean radius \sim 4/1. The LAT source, while faint (0.1–100 GeV flux of $1.6 \pm 0.3 \times 10^{-12} \, \mathrm{erg \, s^{-1} \, cm^{-2}}$), is detected at 5.7σ , with a powerlaw photon index of $\Gamma = 2.54 \pm 0.17$. There is no significant evidence for variability either in the formal variability index or in an examination of the light curve in 1 yr bins (Ballet et al. 2020).

Using archival Swift X-ray Telescope (XRT) data (Stroh & Falcone 2013) taken from the Swift/XRT website (Evans et al.

2009), we identified a single prominent X-ray source within the Fermi-LAT error ellipse, with a J2000 (R.A., decl.) of (04:07:31.78, -57:00:25.2) and a 90% uncertainty of 4"5. There is a single cataloged optical source that matches this X-ray source. The Gaia DR2 ICRS position of this source in (R.A., decl.) is (04:07:31.7195, -57:00:25.295), which we take as the best-known position. This match is <1", so well within the uncertainty of the X-ray position, and the follow-up data discussed below prove the X-ray and optical sources are associated with each other. Furthermore, the Gaia DR2 photometry ($G = 20.176 \pm 0.011$ mag), and presence of the optical source in a catalog of candidate variables identified by the Dark Energy Survey (Stringer et al. 2019), both suggested it might be variable, motivating follow-up.

2.2. Optical Spectroscopy

We obtained optical spectroscopy with the Goodman Spectrograph (Clemens et al. 2004) on the Southern Astrophysical Research (SOAR) telescope on parts of six different nights from 2019 November 6 to 2020 January 17. In all cases we used a 400 l mm $^{-1}$ grating with a 0."95 slit, giving a resolution of about 5.6 Å (FWHM). Some of the spectra were obtained with a wavelength range of $\sim\!\!3820\!\!-\!\!7850\,\text{Å},$ while others used a central wavelength with coverage about 1000 Å redder. Each spectrum had an exposure time of 1500 s. The spectra were all reduced and optimally extracted in the normal manner.

We also obtained several spectra with Gemini/Gemini Multi-Object Spectrograph-South (GMOS-S; Program ID: GS-2019B-FT-111) on the nights of 2019 December 30 and 31. On each night three 1200 s exposures were taken. The R400 grating and a 1."0 slit together yielded an FWHM resolution of about 7.2 Å over the wavelength range ~4500–9150 Å. These data were reduced using the Gemini IRAF package (Gemini Observatory & AURA 2016).

2.3. SOAR Photometry

In an effort to detect periodic optical variability associated with the companion, we observed the source with SOAR/Goodman in imaging mode on 2019 December 16 and again on 2020 January 12. On 2019 December 16, which had seeing around 1", we took a series of 180 s exposures, alternating between the Sloan Digital Sky Survey g' and i' filters, while on the second, brighter night, with a median seeing of 0."8, we only observed in i', with a frame time of 120 s. We performed differential aperture photometry with respect to a set of nearby nonvarying stars, and calibrated to magnitudes from the Dark Energy Survey (Abbott et al. 2018).

2.4. X-Ray Observations

We observed 4FGL J0407.7–5702 on 2020 March 6 with the European Photon Imaging Camera (EPIC) on board the XMM-Newton space telescope. A total livetime of ~22 ks was achieved. Data were reduced using the Science Analysis Software (SAS) data reduction package, version 18.0.0. We used a circular source extraction region of radius 30" centered on J0407.7–5702 and a local background extraction region with an area three times larger. Exposure time intervals of high particle backgrounds were excluded. Standard flagging criteria FLAG = 0, plus #XMMEA_EP and #XMMEA_EM (for pn and MOS detectors, respectively), were applied. Additionally, we

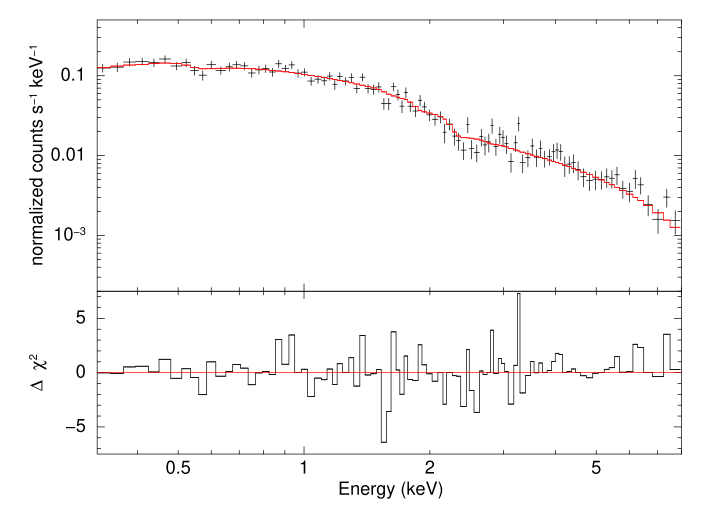


Figure 2. XMM-Newton/EPIC spectrum of 4FGL J0407.7–5702, which is well fit by an absorbed power law with $\Gamma=1.74\pm0.04$.

selected patterns 0–4 for the pn data and 0–12 for the MOS data. Individual background-subtracted spectra were extracted for pn, MOS1, and MOS2 using standard tasks in *xmmselect*. A single combined EPIC spectrum was created using *epicspeccombine* and grouped to at least 20 counts per bin so that Gaussian statistics could be used. For our timing analysis, we used the SAS tasks *evselect* and *epiclccorr* to produce a background-subtracted light curve.

The X-ray source discussed in this paper is the closest source to the center of the Fermi-LAT error ellipse, and has a higher X-ray flux than any other source in the error ellipse by a factor of ~ 20 .

3. Results and Analysis

3.1. X-Ray Spectrum and Mean X-Ray Properties

We began by fitting the XMM-Newton EPIC spectrum with an absorbed power law, as shown in Figure 2. At the Galactic latitude of the source ($b=-44^\circ$) the expected foreground extinction is very low (E(B-V)=0.013; Schlafly & Finkbeiner 2011), with a correspondingly low line-of-sight column density of $N_{\rm H}=1.08\times10^{20}\,{\rm cm}^{-2}$ (HI4PI Collaboration et al. 2016). We find no evidence of additional intrinsic absorption and so fix the $N_{\rm H}$ to this foreground value. This satisfactory model ($\chi^2/{\rm dof}=105.8/96$, p=0.23) results in a best-fit photon index of $\Gamma=1.74\pm0.04$, with an unabsorbed 0.5–10 (1–10) keV flux of 4.16 ± 0.17 (3.47 ± 0.17) $\times 10^{-13}\,{\rm erg\,s}^{-1}\,{\rm cm}^{-2}$. At a reference distance of 7 kpc (see Section 3.5), this flux corresponds to a 0.5–10 keV X-ray luminosity of 2.4 ($d/7\,{\rm kpc})^2\times10^{33}\,{\rm erg\,s}^{-1}$.

We also experimented with adding a blackbody component to the model. However, we found only a marginal improvement $(\chi^2/\text{dof}=101.6/94)$ in the fit, with an F-test probability of p=0.15. As expected, in this fit, the added blackbody component $(kT=0.17\pm0.05~\text{keV})$ results in a slightly harder power-law component $(\Gamma=1.63\pm0.10)$, but the blackbody contributes only $\sim\!5\%$ to the unabsorbed 0.5–10 keV flux. For this two-component model, the unabsorbed 0.5–10 (1–10) keV flux is $4.3\pm0.2~(3.6\pm0.2)\times10^{-13}~\text{erg s}^{-1}~\text{cm}^{-2}$. Given the weak $(<\!2\sigma)$ evidence for a thermal component and its minimal effect on the total flux, we prefer the simpler power-law model, but note that some small thermal contribution could be present.

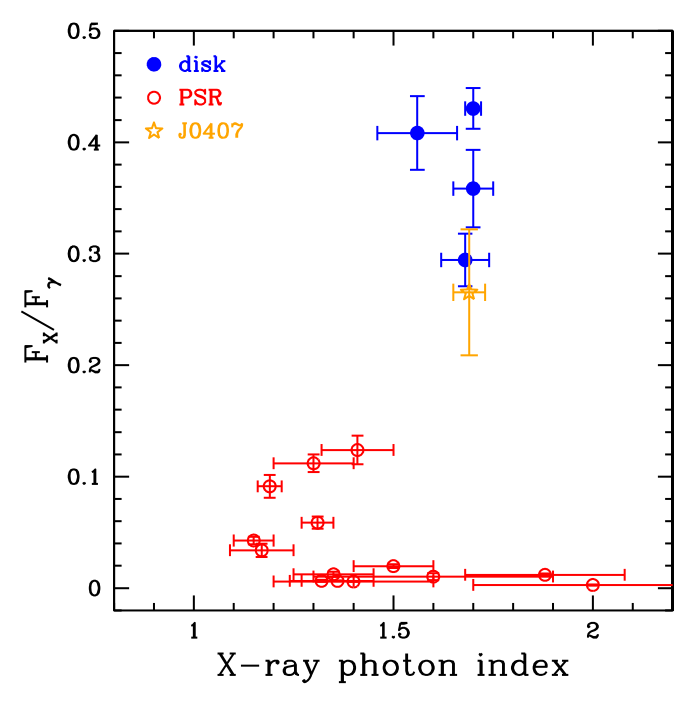


Figure 3. Ratio of X-ray (0.5–10 keV) to γ -ray (0.1–100 GeV) flux vs. X-ray photon index for tMSPs or candidates in the subluminous disk state (filled blue circles) and redbacks or tMSPs in the pulsar state (open red circles). The location of 4FGL J0407.7–5702 (orange star) is consistent with a classification as a disk-state tMSP. The γ -ray fluxes are from Ballet et al. (2020) and the X-ray fluxes from the compilation of Strader et al. (2019), except for PSR J1023+0038 (Bogdanov et al. 2011, 2015; Stappers et al. 2014), XSS J12270–4859 (Linares 2014; Johnson et al. 2015), and the new redback candidate 4FGL J2333.1–5527 (Swihart et al. 2020). The X-ray photon indices are from the compilations of Linares (2014) and Lee et al. (2018) or the literature (Bogdanov et al. 2011, 2015; Bogdanov 2016; Li et al. 2016, 2018, 2020; Strader et al. 2016; Halpern et al. 2017; Al Noori et al. 2018; Cho et al. 2018; Gentile 2018; Linares 2018; Swihart et al. 2018, 2020; de Martino et al. 2020).

The hard power law, with $\Gamma=1.74\pm0.04$, matches the X-ray spectrum of PSR J1023+0038 (Bogdanov et al. 2015) in the subluminous disk state as well as that of the tMSP candidates J1544.6–1125 (Bogdanov 2016), 3FGL J0427.9–6704 (Strader et al. 2016; Li et al. 2020), and CXOU J110926.4–650224 (Coti Zelati et al. 2019). A similar hard power law has also been observed for quiescent accreting millisecond pulsars such as SAX J1808.4–3658 (Heinke et al. 2009), though such sources do not show an optical disk nor the extreme variability observed for tMSPs in the subluminous disk state.

3.1.1. Relative X-Ray and \gamma-Ray Flux

Since the distance to 4FGL J0407.7–5702 is not known, we cannot effectively assess whether its X-ray luminosity supports an identification as a candidate tMSP. Nevertheless, here we show that the ratio of its X-ray and γ -ray fluxes—a distance-independent quantity—does indeed support this classification.

The X-ray (0.5–10 keV) to γ -ray (0.1–100 GeV) flux ratio for 4FGL J0407.7–5702 is $F_{\rm X}/F_{\gamma}=0.26\pm0.06$. In Figure 3 we show this ratio, plotted against the X-ray photon index from a power-law spectral fit, for 4FGL-detected sources in the subluminous disk state⁴ (PSR J1023+03038, XSS

J12270–4859, 3FGL J1544.6–1125, and 3FGL J0427.9–6704) as well as all redbacks in the pulsar state that appear in the 4FGL catalog and that have well-measured photon indices (uncertainties <0.5).

Figure 3 shows that the four confirmed or candidate field tMSPs in the subluminous disk state have $F_{\rm X}/F_{\gamma}$ in the range 0.29–0.43. This can be compared to a median value of 0.012 for redbacks in the pulsar state, and a maximum of $F_{\rm X}/F_{\gamma}\sim 0.12$ (for 1FGL J1417.7–4407, which has an evolved companion and perhaps an unusually luminous intrabinary shock). 4FGL J0407.7–5702 has an $F_{\rm X}/F_{\gamma}$ value consistent within the uncertainties with that observed for tMSPs, supporting its classification as such. By contrast, the recently discovered binary 4FGL J0935.3+0901, whose optical and X-ray data alone do not allow a clear classification (Wang et al. 2020), has $F_{\rm X}/F_{\gamma}\sim 0.02$, suggesting it is much more likely to be in the pulsar state than the subluminous disk state.

The transitions of PSR J1023+03038 and XSS J12270-4859 show the proximate reason for this difference between the disk and pulsar states: in the disk state their 0.1-100 GeV γ -ray fluxes are higher by only a factor of \sim 3-6 compared to the pulsar state (Stappers et al. 2014; Johnson et al. 2015), but their 0.5-10 keV X-ray fluxes are higher by a factor of \sim 25-30 (Bogdanov et al. 2011, 2015; Linares et al. 2014; de Martino et al. 2020). Whether this difference holds for other tMSPs awaits future observed transitions, but the location of candidate disk-state tMSPs in the same region as confirmed tMSPs is suggestive of it.

If tMSPs do indeed all have relatively high values of $F_{\rm X}/F_{\gamma}$, this has ramifications for the identification of new tMSPs among currently unassociated Fermi γ -ray sources. New sources in the 10 yr catalog have typical 0.1–100 GeV fluxes of $1-3\times 10^{-12}~{\rm erg\,s^{-1}\,cm^{-2}}$ (Ballet et al. 2020). For typical tMSP-like values of $F_{\rm X}/F_{\gamma}$, the corresponding 0.5–10 keV fluxes are $F_{\rm X}\sim 3\times 10^{-13}$ to $10^{-12}\,{\rm erg\,s^{-1}\,cm^{-2}}$, detectable with Swift/XRT for short exposure times of 1–2 ks even in the presence of moderate foreground extinction ($N_{\rm H} \lesssim 10^{22}~{\rm cm}^{-2}$). The expected all-sky X-ray sensitivity of eROSITA is similar (Merloni et al. 2012). The implication is that for essentially any tMSP in the subluminous disk state detected as a Fermi GeV source, an X-ray counterpart should be readily identifiable even in shallow data. This is unlike the case for redbacks or black widows, which can have much fainter X-ray counterparts. Since typical Fermi error ellipses can contain a number of unrelated X-ray sources, the mere existence of a candidate X-ray counterpart cannot be used to provide a definitive classification, but the absence of such a counterpart would disfavor the identification of the source as a tMSP.

Figure 3 also shows that, consistent with previous work (e.g., Linares 2014), the tMSPs or candidates in the disk state have $\Gamma \sim 1.7$, but that redbacks show a wide range of photon indices, in part depending on the strength of the intrabinary shock. Therefore, the X-ray photon index can only give indicative, but not conclusive, information about the classification of a candidate tMSP.

3.1.2. ROSAT

There is a faint $(0.020 \pm 0.008\,\mathrm{ct\,s^{-1}})$ ROSAT source, 2RXS J040730.2–570024 (Boller et al. 2016), with a catalog position 11" from that of the optical/X-ray counterpart to 4FGL J0407.7–5702. Assuming the best-fit XMM spectral model, this ROSAT count rate is equivalent to a 0.5–10 keV

 $^{^{4}}$ CXOU J110926.4–650224 was associated with a tentative 8 yr source (FL8Y J1109.8–6500) that is not in the official 4FGL catalog. Using FL8Y, $F_{\rm X}/F_{\gamma}=0.67\pm0.27$.

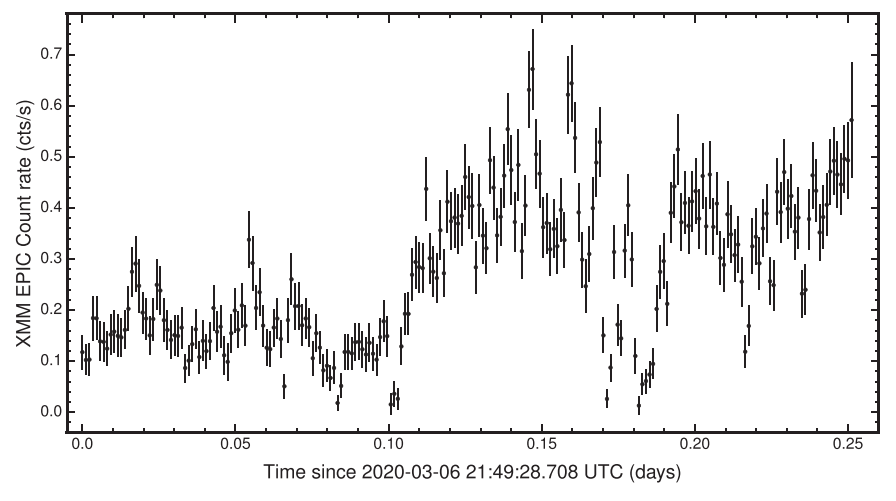


Figure 4. Background-subtracted and barycentric-corrected XMM-Newton EPIC light curve of 4FGL J0407.7-5702 in the 0.2-10 keV band, binned in 100 s bins.

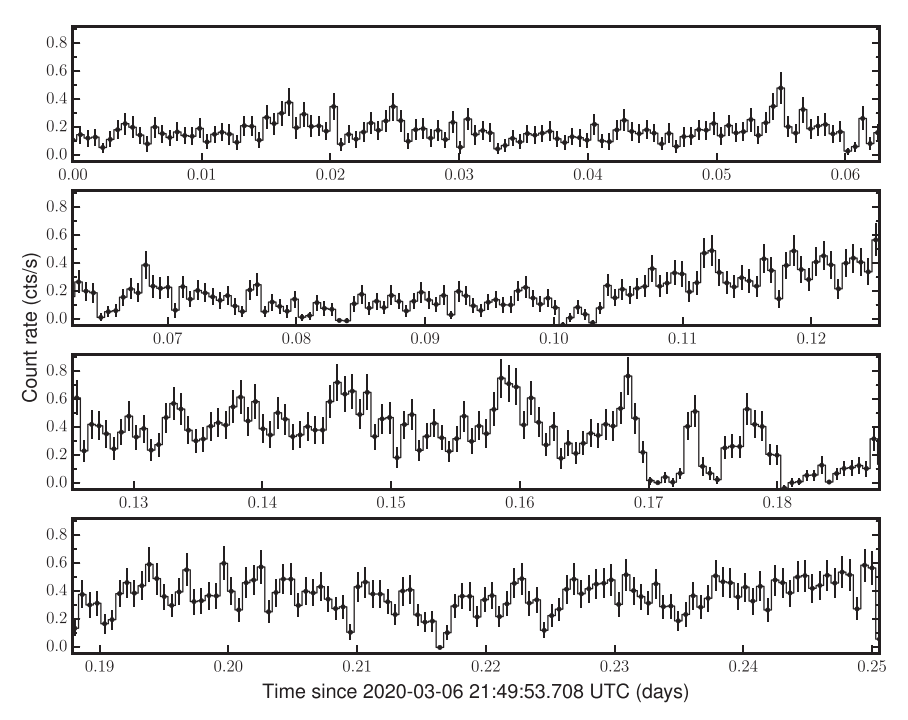


Figure 5. The same data as in Figure 4, but instead with finer 50 s bins.

flux of $(3.6 \pm 1.4) \times 10^{-13} \, \text{erg s}^{-1} \, \text{cm}^{-2}$, identical to the XMM flux within the uncertainties. Given how similar these fluxes are, the lack of another XMM X-ray source within \sim 45" of the target, and the poor astrometry expected for faint ROSAT sources, we think it is likely that 2RXS J040730.2-570024 is the same as the XMM source despite the astrometric offset. If so, this implies that 4FGL J0407.7-5702 was in a similar spectral state in 1990-1991 to 2019–2020. While the γ -ray source is faint, there is no evidence for significant γ -ray variability since 2008 (Ballet et al. 2020), and hence no reason to believe a transition occurred in this time interval. The constraints on a possible "full" X-ray outburst are weak: at our inferred range of likely distances, an outburst to $L_{\rm X} \sim 10^{36}\,{\rm erg\,s^{-1}}$ would have only reached a few milliCrab, so its discovery by all-sky X-ray monitors would have been borderline.

3.2. X-Ray Light Curve

The background-subtracted and barycentric-corrected XMM-Newton EPIC 0.2–10 keV light curve, shown separately in 100 s bins (Figure 4) and 50 s bins (Figure 5), display clear short-term variability over the 21.7 ks exposure. A histogram of the finer 50 s binned light curve shows a bimodal distribution (Figure 6). For exploratory analysis in this section, we use this figure to guide a preliminary division of the light curve into three separate flux levels: low (0.0–0.3 ct s $^{-1}$), medium (0.3–0.6 ct s $^{-1}$), and flare (>0.6 ct s $^{-1}$). The average 0.2–10 keV count rates is 0.204 \pm 0.003 ct s $^{-1}$.

4FGL J0407.7–5702 spent a majority of the observation at the low (\sim 60% of the time) or medium (\sim 37%) flux levels, with occasional flares (\sim 2%–3%). Given that fast, frequent "mode switching" between the low and high modes is observed clearly in PSR J1023+0038, XSS J12270–4859, and 3FGL J1544.6–1125 (Linares 2014; Bogdanov et al. 2015; Bogdanov & Halpern 2015), it is tempting to associate the low and

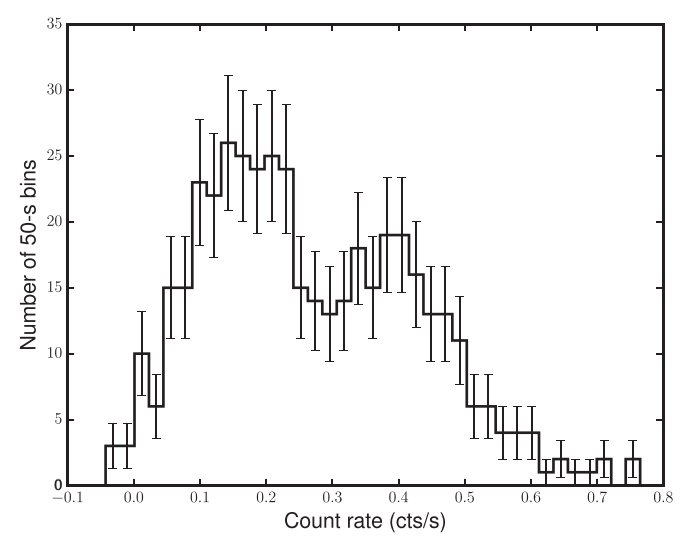


Figure 6. Distribution of count rates from the 50 s binned background-subtracted XMM-Newton EPIC light curve. We define the following regions according to their flux levels: low $(0.0-0.3 \text{ ct s}^{-1})$, medium $(0.3-0.6 \text{ ct s}^{-1})$, and flare $(>0.6 \text{ ct s}^{-1})$.

medium count levels observed for 4FGL J0407.7–5702 with these well-studied modes.

However, there are several reasons to think this simple interpretation is not correct. First, in these other systems the flux difference between the low and high modes is large (a factor of \sim 5–10), while in 4FGL J0407.7–5702 the difference is only a factor of \sim 2–2.5. Another difference is that in the other tMSPs and candidates the binary is in the high mode for the majority (\gtrsim 75%) of the time, compared to <40% here.

A careful examination of Figure 5 shows that the system does indeed make excursions to a count rate much fainter than the broad, low flux level identified in Figure 6. The most extensive of these is around 0.17 d after the light-curve start, where the binary has a flat-bottomed light curve with a mean count rate of 0.027 ± 0.014 ct s⁻¹. This is a factor of \sim 7–8 fainter than the average count rate over the whole data set, and equivalent to a 0.5–10 keV X-ray luminosity of $(3.2 \pm 1.6) (d/7 \, \text{kpc})^2 \times 10^{32} \, \text{erg s}^{-1}$. We suggest it might be more accurate to view this rarer state as the true "low mode" and both the peaks at 0.15–0.2 ct s⁻¹ and 0.4 ct s⁻¹ as manifestations of the same "high mode."

Indeed, from a phenomenological point of view the X-ray light curve most closely resembles that of the tMSP candidate CXOU J110926.4–650224, which shows occasional low modes but less pronounced bimodality over its entire light curve than some of the other tMSPs (Coti Zelati et al. 2019). It may also be the case that tMSPs show a broader set of behaviors than simple mode switching; for example, the tMSP candidate 3FGL J0427.9–6704 shows bright γ -ray and radio continuum emission as well as a disk, appears to spend most of its time in an X-ray flare mode, with no consistent stable low or high modes (Li et al. 2020).

3.3. Optical Spectroscopy

All of the SOAR spectra show the same features: a blue continuum with superimposed emission lines from H I, He I, and the 4686 Å line of He II. The emission lines are resolved, with a mean resolution-corrected FWHM of 516 \pm 21 km s $^{-1}$ for $H\alpha$ measured among the different epochs. A mean of the

stronger He I lines is yet broader at \sim 670 km s⁻¹, and the He II 4686 Å line is double-peaked with an FWHM \sim 830 km s⁻¹. This trend of increasing FWHM is consistent with the idea that the H emission is primarily from the outer disk, with He I and then He II dominated by regions progressively closer to the compact object (Figure 7).

There are no photospheric absorption features apparent either visually or in a cross-correlation with templates of the expected spectral types of the likely low-mass secondary. We obtained the Gemini spectra in the hope of uncovering faint absorption features in higher signal-to-noise spectra, but did not find any in these data either.

We next attempted to constrain the orbital period through motion of the emission lines. While the different epochs of data do show evidence for modest variations in the wavelengths of the emission lines (of order $\sim 20-30~{\rm km~s}^{-1}$), these did not phase on any readily identifiable orbital period.

Qualitatively, in terms of the presence of emission lines and their relative strengths, the 4FGL J0407.7–5702 spectra are very similar to those of the confirmed tMSP PSR J1023+0038 in its disk state and to the candidate tMSP 3FGL J1544.6–1125, and consistent overall with the optical spectra expected for an accretion disk around a compact object.

Under the assumption that the emission lines do arise in an accretion disk around a neutron star, their relatively narrow FWHM hints at a more face-on inclination. For example, the neutron star low-mass X-ray binary Cen X-4 has a H α FWHM of 678 \pm 48 km s $^{-1}$ (Casares 2015) and an inclination of $35^{+5}_{-4}^{\circ}$ (Hammerstein et al. 2018), while 3FGL J1544.6–1125 has an FWHM of $\sim\!330$ km s $^{-1}$ and an inclination of $5^{\circ}\!-\!8^{\circ}$ (Britt et al. 2017). 4FGL J0407.7–5702, with a H α FWHM of 516 ± 21 km s $^{-1}$, likely has an inclination within this broad range of face-on values, assuming its orbital period and primary mass are not too dissimilar from typical neutron star low-mass X-ray binaries.

3.4. Optical Photometry

The SOAR optical (g' and i') light curves from our two epochs are shown in Figure 8. In the 2019 December epoch, with g' and i' data taken over three hours, the light curves in both filters show aperiodic, seemingly stochastic variations. The short timescale variations in both filters are reminiscent of the "flickering" seen in the light curve of PSR J1023+0338 while in its subluminous disk state (Kennedy et al. 2018).

The 2020 January epoch, with data only in i', extends over a longer time span of nearly 6 hr. The variability is qualitatively different than the earlier optical photometry. By eye there is some evidence for periodic variability in the repeating distinct maxima (Figure 8), but these do not repeat regularly: the second and third peaks are separated by ~ 1.1 hr, and the third and fourth by ~ 1.7 hr. A Lomb–Scargle periodogram analysis of this light curve does not show evidence for a significant peak (with only a weak, insignificant peak at 56 minutes). It is unlikely that any of these timescales represent the orbital period of the binary; of the known redbacks, the system with the shortest well-measured orbital period is PSR J1622–0315, at 3.9 hr (Sanpa-arsa 2016). It is unknown whether all the tMSP candidates are indeed redbacks and hence whether less massive donors and hence shorter periods might be possible.

Instead, the 2020 January 13 light curve more closely resembles the "limit cycle" behavior present most clearly in the tMSP candidate 3FGL J1544.6–1125, which shows short

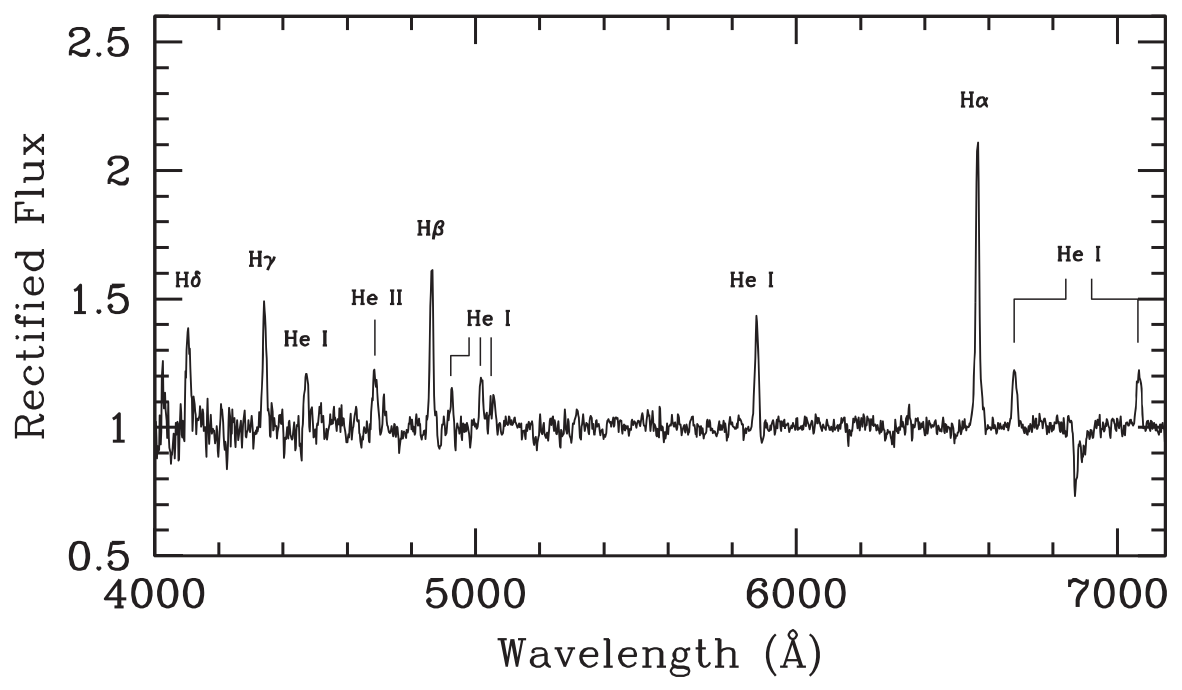


Figure 7. Rectified coadded SOAR optical spectra of 4FGL J0407.7–5702. The main Balmer and He II lines are marked. The spectrum is that of a typical accretion disk, with the only significant absorption lines telluric.

(The data used to create this figure are available.)

timescale variations confined between minimum and maximum values separated by ~ 0.5 mag (Bogdanov & Halpern 2015), as opposed to random flickering. Similar behavior is also observed in XSS J12270–4859 (Pretorius 2009; de Martino et al. 2010) and PSR J1023+0038 (Bond et al. 2002; Bogdanov et al. 2015; Kennedy et al. 2018), although in these systems modulation on the orbital period is also observed, superimposed on the shorter timescale variations. Such orbital variations, if present, might be harder to observe for 4FGL J0407.7–5702 given its likely face-on orientation (Section 3.3).

3.5. Distance

Since 4FGL J0407.7–5702 does not have a significant Gaia DR2 parallax ($\varpi = -0.37 \pm 0.48$ mas; Gaia Collaboration et al. 2018), nor the possibility of modeling the flux from a Roche lobe–filling secondary, we must use alternative methods to constrain its distance. To estimate the most likely distance, we proceed under the assumption that it has intrinsic properties similar to the known tMSPs.

First, we consider its γ -ray and X-ray flux in the context of the four known or candidate tMSPs that have reasonably well-constrained distances. From the compilation of Strader et al. (2019), the 0.1–100 GeV γ -ray luminosities of these four sources range from $6\times 10^{33}\,\mathrm{erg\,s^{-1}}$ to $2.4\times 10^{34}\,\mathrm{erg\,s^{-1}}$, which given the flux of 4FGL J0407.7–5702 would imply a distance in the range 5.6–11.2 kpc. Similarly, given mean 0.5–10 keV X-ray luminosities of $2.4\times 10^{33}\,\mathrm{erg\,s^{-1}}$ to $7.7\times 10^{33}\,\mathrm{erg\,s^{-1}}$ for these sources, the implied X-ray distance is in the range 6.9–12.5 kpc.

As a third estimate we consider the Gaia photometry for the three sources with well-constrained distances and that have been in the disk state for the Gaia era: PSR J1023+0038, 3FGL J1544.6-1125, and 3FGL J0427.9-6704. We focus on the $G_{\rm BP}$ photometry under the hypothesis that this region of the

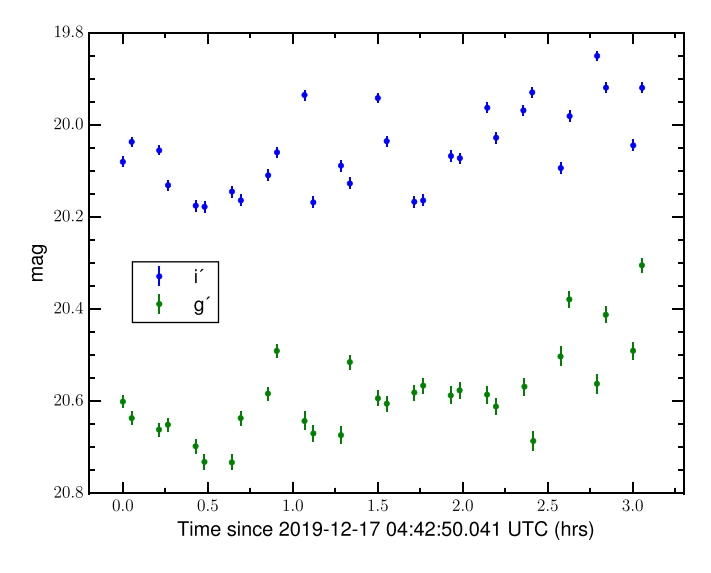
spectrum is more likely to be disk-dominated, and under the ansatz that given the vaguely similar X-ray luminosities and periods of these sources their blue disk luminosities might also be similar. Using Gaia DR2 (Gaia Collaboration et al. 2018), accounting for foreground reddening (Schlafly & Finkbeiner 2011; Marigo et al. 2017), and the distances from Strader et al. (2019), the range of absolute $M_{G_{\rm BP}}$ for this small sample of objects is indeed small, from $M_{G_{\rm BP}} \sim 5.6$ –6.0. Given $G_{\rm BP,0} = 20.22 \pm 0.09$ for 4FGL J0407.7–5702, the implied range of optical distances is 7.2–8.3 kpc. The systematic uncertainties associated with this optical distance estimate are likely much larger than even those for the X-ray and γ -ray distances, but nevertheless, these values fall within the the range of the high-energy distances.

Above and for the remainder of the paper we quote a reference distance of 7 kpc, but emphasize that this is not a best-fit distance estimate of the binary and that the uncertainty on the distance is substantial. We are more secure in saying that if 4FGL J0407.7–5702 has intrinsic properties similar to the other known and candidate tMSPs, then a distance of \lesssim 5 kpc is disfavored.

4. Discussion and Conclusions

We have shown that the brightest X-ray source within the error ellipse of the Fermi-LAT γ -ray source 4FGL J0407.7–5702 has an X-ray light curve and spectrum consistent with known and strong candidate tMSPs in the subluminous disk state. Photometry and spectroscopy of the optical counterpart to this X-ray source provides compelling support for this scenario, as does the high ratio of X-ray to γ -ray flux.

A definitive classification as a tMSP would require an observed transition to the pulsar state, which could be suggested by γ -ray, X-ray, and optical monitoring of the source. Nonetheless, our conclusion could be strengthened with



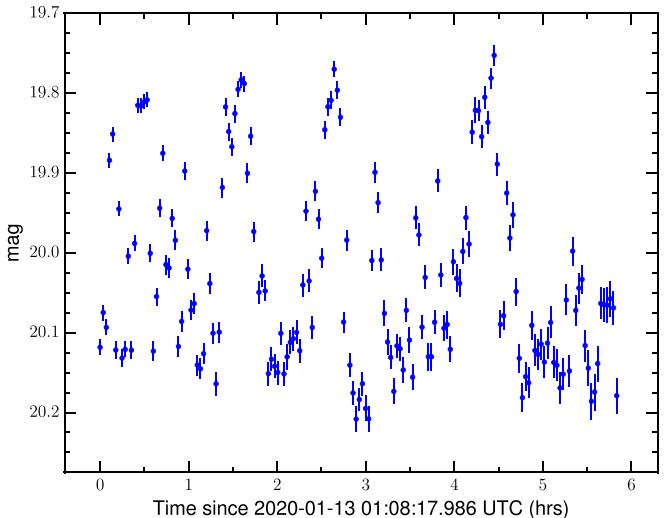


Figure 8. Top: SOAR g' and i' optical photometry of 4FGL J0407.7–5702, taken on 2019 December 17. Bottom: SOAR i' photometry from 2020 January 13, showing the limit cycle behavior discussed in the text.

(The data used to create this figure are available.)

additional data in the present state. The most straightforward of these would be longer X-ray observations with XMM-Newton or Chandra, which could reveal whether the hints of mode switching behavior discussed above are borne out with more data. X-ray timing observations with one of these telescopes, or perhaps with NICER, could in principle reveal if the system shows X-ray pulsations similar to PSR J1023+0038 in the subluminous disk state (Jaodand et al. 2016), though in the absence of radio ephemerides such detections are challenging. Alternatively, it is possible that 4FGL J0407.7–5702 shows X-ray phenomenology beyond mode switching, not unlike 3FGL J0427.9–6704, supporting a wider range of behaviors for these systems.

Another useful measurement would be the orbital period of the binary, which we could not determine using our optical photometry or spectroscopy. Rapid cadence optical photometry, or photometry or spectroscopy in the near-infrared (where the contribution of the donor star might be more observable compared to the disk) are potential alternative approaches. Since PSR J1023+0038 (Deller et al. 2015), XSS J12270–4859 (Hill et al. 2011), 3FGL J1544.6–1125 (Jaodand 2019), and 3FGL J0427.9–6704 (Li et al. 2020) all show radio continuum emission in their subluminous disk states, the radio behavior of 4FGL J0407.7–5702 could strengthen its tentative classification as a candidate tMSP. The plausibility of a detection depends on its unknown distance and radio behavior: if at 7 kpc, it would be well detectable if at the 5 GHz radio luminosity of 3FGL J0427.9–6704 (predicted flux density of \sim 31 μ Jy), marginal if as luminous as XSS J12270–4859 or 3FGL J1544.6–1125, and very difficult if akin to PSR J1023+0038 (mean flux density \sim 2–6 μ Jy, though with occasional brighter flares).

Under the assumption that 4FGL J0407.7–5702 has a luminosity comparable to previously studied tMSPs in the X-ray, γ -ray, or optical, we found the most likely distance to lie in the range \sim 6–13 kpc, with a consensus value more toward the lower end of that range. While the uncertainty in these estimates is substantial, together they suggest that 4FGL J0407.7–5702 is the most distant known candidate field tMSP to date. It is possible, though not certain, that an end-of-mission Gaia parallax for this source might be available, which would allow the crucial determination of its X-ray luminosity.

Finally, we highlight the emerging evidence that the ratio of X-ray to γ -ray flux $(F_{\rm X}/F_{\gamma})$ could help to identify candidate tMSPs in the subluminous disk state and separate them from the more common redbacks or black widows when good distance constraints are not available. Since the increasingly deep Fermi-LAT catalogs are enabling the study of more distant millisecond pulsar binaries, such techniques may see increasing relevance in follow-up studies in the coming years.

We acknowledge a helpful and thoughtful report from an anonymous referee. We also acknowledge support from NSF grant AST-1714825 and the Packard Foundation.

This work is based on observations obtained with XMM-Newton an ESA science mission with instruments and contributions directly funded by ESA Member States and NASA.

Based on observations obtained at the Southern Astrophysical Research (SOAR) telescope, which is a joint project of the Ministério da Ciência, Tecnologia, Inovações e Comunicações (MCTIC) do Brasil, the U.S. National Optical Astronomy Observatory (NOAO), the University of North Carolina at Chapel Hill (UNC), and Michigan State University (MSU).

Based on observations obtained at the international Gemini Observatory, a program of NSF's OIR Lab, which is managed by the Association of Universities for Research in Astronomy (AURA) under a cooperative agreement with the National Science Foundation. On behalf of the Gemini Observatory partnership: the National Science Foundation (United States), National Research Council (Canada), Agencia Nacional de Investigación y Desarrollo (Chile), Ministerio de Ciencia, Tecnología e Innovación (Argentina), Ministério da Ciência, Tecnologia, Inovações e Comunicações (Brazil), and Korea Astronomy and Space Science Institute (Republic of Korea).

Software: IRAF (Tody 1986; Gemini Observatory & AURA 2016), SAS (v18.0.0; Gabriel et al. 2004), Astropy (Astropy Collaboration et al. 2013).

ORCID iDs

Jessie M. Miller https://orcid.org/0000-0001-8840-922X

Samuel J. Swihart https://orcid.org/0000-0003-1699-8867
Jay Strader https://orcid.org/0000-0002-1468-9668
Ryan Urquhart https://orcid.org/0000-0003-1814-8620
Elias Aydi https://orcid.org/0000-0001-8525-3442
Laura Chomiuk https://orcid.org/0000-0002-8400-3705
Kristen C. Dage https://orcid.org/0000-0002-8532-4025
Adam Kawash https://orcid.org/0000-0003-0071-1622
Laura Shishkovsky https://orcid.org/0000-0003-0286-7858
Kirill V. Sokolovsky https://orcid.org/0000-0001-5991-6863

References

```
Abbott, T. M. C., Abdalla, F. B., Allam, S., et al. 2018, ApJS, 239, 18
Al Noori, H., Roberts, M. S. E., Torres, R. A., et al. 2018, ApJ, 861, 89
Ambrosino, F., Papitto, A., Stella, L., et al. 2017, NatAs, 1, 854
Archibald, A. M., Bogdanov, S., Patruno, A., et al. 2015, ApJ, 807, 62
Archibald, A. M., Kaspi, V. M., Bogdanov, S., et al. 2010, ApJ, 722, 88
Archibald, A. M., Stairs, I. H., Ransom, S. M., et al. 2009, Sci, 324, 1411
Astropy Collaboration, Robitaille, T. P., Tollerud, E. J., et al. 2013, A&A,
   558, A33
Ballet, J., Burnett, T. H., Digel, S. W., & Lott, B. 2020, arXiv:2005.11208
Bassa, C. G., Patruno, A., Hessels, J. W. T., et al. 2014, MNRAS, 441, 1825
Bogdanov, S. 2016, ApJ, 826, 28
Bogdanov, S., Archibald, A. M., Bassa, C., et al. 2015, ApJ, 806, 148
Bogdanov, S., Archibald, A. M., Hessels, J. W. T., et al. 2011, ApJ, 742, 97
Bogdanov, S., Deller, A. T., Miller-Jones, J. C. A., et al. 2018, ApJ, 856, 54
Bogdanov, S., & Halpern, J. P. 2015, ApJL, 803, L27
Boller, T., Freyberg, M. J., Trümper, J., et al. 2016, A&A, 588, A103
Bond, H. E., White, R. L., Becker, R. H., & O'Brien, M. S. 2002, PASP,
   114, 1359
Britt, C. T., Strader, J., Chomiuk, L., et al. 2017, ApJ, 849, 21
Casares, J. 2015, ApJ, 808, 80
Cho, P. B., Halpern, J. P., & Bogdanov, S. 2018, ApJ, 866, 71
Clemens, J. C., Crain, J. A., & Anderson, R. 2004, Proc. SPIE, 5492, 331
Coti Zelati, F., Papitto, A., de Martino, D., et al. 2019, A&A, 622, A211
D'Angelo, C. R., & Spruit, H. C. 2012, MNRAS, 420, 416
de Martino, D., Belloni, T., Falanga, M., et al. 2013, A&A, 550, A89
de Martino, D., Casares, J., Mason, E., et al. 2014, MNRAS, 444, 3004
de Martino, D., Falanga, M., Bonnet-Bidaud, J. M., et al. 2010, A&A,
   515, A25
de Martino, D., Papitto, A., Belloni, T., et al. 2015, MNRAS, 454, 2190
de Martino, D., Papitto, A., Burgay, M., et al. 2020, MNRAS, 492, 5607
Degenaar, N., Wijnands, R., Reynolds, M. T., et al. 2014, ApJ, 792, 109
Deller, A. T., Moldon, J., Miller-Jones, J. C. A., et al. 2015, ApJ, 809, 13
Evans, P. A., Beardmore, A. P., Page, K. L., et al. 2009, MNRAS, 397, 1177
Gabriel, C., Denby, M., Fyfe, D. J., et al. 2004, in ASP Conf. Ser. 314,
   Astronomical Data Analysis Software and Systems (ADASS) XIII, ed.
   F. Ochsenbein, M. G. Allen, & D. Egret (San Francisco, CA: ASP), 759
Gaia Collaboration, Brown, A. G. A., Vallenari, A., et al. 2018, A&A, 616, A1
Gemini Observatory AURA 2016, Gemini IRAF: Data Reduction Software for
   the Gemini Telescopes, v2.16, Astrophysics Source Code Library,
Gentile, P. A. 2018, PhD thesis, West Virginia Univ.
```

```
Halpern, J. P., Bogdanov, S., & Thorstensen, J. R. 2017, ApJ, 838, 124
Hammerstein, E. K., Cackett, E. M., Reynolds, M. T., & Miller, J. M. 2018,
   MNRAS, 478, 4317
Heinke, C. O., Bahramian, A., Degenaar, N., & Wijnand s, R. 2015, MNRAS,
  447, 3034
Heinke, C. O., Jonker, P. G., Wijnands, R., Deloye, C. J., & Taam, R. E. 2009,
    pJ, 691, 1035
Hill, A. B., Szostek, A., Corbel, S., et al. 2011, MNRAS, 415, 235
HI4PI Collaboration, Ben Bekhti, N., Flöer, L., et al. 2016, A&A, 594, A116
Jaodand, A., Archibald, A. M., Hessels, J. W. T., et al. 2016, ApJ, 830, 122
Jaodand, A. D. 2019, PhD thesis, Univ. Amsterdam
Johnson, T. J., Ray, P. S., Roy, J., et al. 2015, ApJ, 806, 91
Kennedy, M. R., Clark, C. J., Voisin, G., & Breton, R. P. 2018, MNRAS,
  477, 1120
Lee, J., Hui, C. Y., Takata, J., et al. 2018, ApJ, 864, 23
Li, K.-L., Hou, X., Strader, J., et al. 2018, ApJ, 863, 194
Li, K.-L., Kong, A. K. H., Hou, X., et al. 2016, ApJ, 833, 143
Li, K.-L., Strader, J., Miller-Jones, J. C. A., Heinke, C. O., & Chomiuk, L.
  2020, ApJ, 895, 89
Linares, M. 2014, ApJ, 795, 72
Linares, M. 2018, MNRAS, 473, L50
Linares, M., Bahramian, A., Heinke, C., et al. 2014, MNRAS, 438, 251
Marigo, P., Girardi, L., Bressan, A., et al. 2017, ApJ, 835, 77
Merloni, A., Predehl, P., Becker, W., et al. 2012, arXiv:1209.3114
Papitto, A., Ambrosino, F., Stella, L., et al. 2019, ApJ, 882, 104
Papitto, A., de Martino, D., Belloni, T. M., et al. 2015, MNRAS, 449, L26
Papitto, A., Ferrigno, C., Bozzo, E., et al. 2013, Natur, 501, 517
Papitto, A., & Torres, D. F. 2015, ApJ, 807, 33
Patruno, A., Archibald, A. M., Hessels, J. W. T., et al. 2014, ApJL, 781, L3
Patruno, A., Haskell, B., & Andersson, N. 2017, ApJ, 850, 106
Patruno, A., & Watts, A. L. 2012, arXiv:1206.2727
Pretorius, M. L. 2009, MNRAS, 395, 386
Ray, P. S., Abdo, A. A., Parent, D., et al. 2012, arXiv:1205.3089
Roberts, M. S. E. 2013, in IAU Symp. 291, Neutron Stars and Pulsars:
  Challenges and Opportunities after 80 years, ed. J. van Leeuwen
  (Cambridge: Cambridge Univ. Press), 127
Roberts, M. S. E., Mclaughlin, M. A., Gentile, P., et al. 2014, AN, 335, 313
Roy, J., Ray, P. S., Bhattacharyya, B., et al. 2015, ApJL, 800, L12
Sanpa-arsa, S. 2016, PhD thesis, Univ. Virginia
Schlafly, E. F., & Finkbeiner, D. P. 2011, ApJ, 737, 103
Stappers, B. W., Archibald, A. M., Hessels, J. W. T., et al. 2014, ApJ, 790, 39
Strader, J., Li, K.-L., Chomiuk, L., et al. 2016, ApJ, 831, 89
Strader, J., Swihart, S., Chomiuk, L., et al. 2019, ApJ, 872, 42
Stringer, K. M., Long, J. P., Macri, L. M., et al. 2019, AJ, 158, 16
Stroh, M. C., & Falcone, A. D. 2013, ApJS, 207, 28
Swihart, S. J., Strader, J., Shishkovsky, L., et al. 2018, ApJ, 866, 83
Swihart, S. J., Strader, J., Urquhart, R., et al. 2020, ApJ, 892, 21
Takata, J., Li, K. L., Leung, G. C. K., et al. 2014, ApJ, 785, 131
Thorstensen, J. R., & Armstrong, E. 2005, AJ, 130, 759
Tody, D. 1986, Proc. SPIE, 627, 733
Torres, D. F., Ji, L., Li, J., et al. 2017, ApJ, 836, 68
Torres, D. F., & Li, J. 2020, arXiv:2004.03128
van Paradijs, J. 1998, arXiv:astro-ph/9802177
Veledina, A., Nättilä, J., & Beloborodov, A. M. 2019, ApJ, 884, 144
Wang, Z., Xing, Y., Zhang, J., et al. 2020, MNRAS, 493, 4845
```